

m⁶A RNA Modification Controls Cell Fate Transition in Mammalian Embryonic Stem Cells

Pedro J. Batista,^{1,9} Benoit Molinie,^{2,9} Jinkai Wang,^{3,9} Kun Qu,¹ Jiajing Zhang,¹ Lingjie Li,¹ Donna M. Bouley,⁴ Ernesto Lujan,^{5,6} Bahareh Haddad,⁵ Kaveh Daneshvar,² Ava C. Carter,¹ Ryan A. Flynn,¹ Chan Zhou,² Kok-Seong Lim,⁷ Peter Dedon,⁷ Marius Wernig,⁵ Alan C. Mullen,^{2,8} Yi Xing,^{3,*} Cosmas C. Giallourakis,^{2,8,*} and Howard Y. Chang^{1,*}

¹Howard Hughes Medical Institute and Program in Epithelial Biology, Stanford University School of Medicine, Stanford, CA 94305, USA

²Gastrointestinal Unit, Massachusetts General Hospital, Harvard Medical School, Boston, MA 02114, USA

³Department of Microbiology, Immunology, and Molecular Genetics, University of California, Los Angeles, Los Angeles, CA 90095, USA

⁴Department of Comparative Medicine, Stanford University School of Medicine, Stanford, CA 94305, USA

⁵Institute for Stem Cell Biology and Regenerative Medicine and Department of Pathology, Stanford University School of Medicine, Stanford, CA 94305, USA

⁶Department of Genetics, Stanford University School of Medicine, Stanford, CA 94305, USA

⁷Department of Biological Engineering, Massachusetts Institute of Technology, Cambridge, MA 02139, USA

⁸Harvard Stem Cell Institute, Cambridge, MA 02138, USA

⁹Co-first author

*Correspondence: yxing@ucla.edu (Y.X.), cgiallourakis@mgh.harvard.edu (C.C.G.), howchang@stanford.edu (H.Y.C.)

<http://dx.doi.org/10.1016/j.stem.2014.09.019>

SUMMARY

N⁶-methyl-adenosine (m⁶A) is the most abundant modification on messenger RNAs and is linked to human diseases, but its functions in mammalian development are poorly understood. Here we reveal the evolutionary conservation and function of m⁶A by mapping the m⁶A methylome in mouse and human embryonic stem cells. Thousands of messenger and long noncoding RNAs show conserved m⁶A modification, including transcripts encoding core pluripotency transcription factors. m⁶A is enriched over 3' untranslated regions at defined sequence motifs and marks unstable transcripts, including transcripts turned over upon differentiation. Genetic inactivation or depletion of mouse and human *Mettl3*, one of the m⁶A methylases, led to m⁶A erasure on select target genes, prolonged *Nanog* expression upon differentiation, and impaired ESC exit from self-renewal toward differentiation into several lineages in vitro and in vivo. Thus, m⁶A is a mark of transcriptome flexibility required for stem cells to differentiate to specific lineages.

INTRODUCTION

Reversible chemical modifications on messenger RNAs (mRNAs) have emerged as prevalent phenomena that may open a new field of “RNA epigenetics,” where RNA modifications have an impact akin to the diverse roles that DNA modifications play in epigenetics (reviewed by Fu and He, 2012; Sibbritt et al., 2013). N⁶-methyl-adenosine (m⁶A) is the most prevalent modification of mRNAs in somatic cells, and dysregulation of this modification has already been linked to obesity, cancer, and other human diseases (Sibbritt et al., 2013). m⁶A has been

observed in a wide range of organisms, and the methylation complex is conserved across eukaryotes. In budding yeast, the m⁶A methylation program is activated by starvation and required for sporulation. In *Arabidopsis thaliana*, the methylase responsible for m⁶A modification, MTA, is essential for embryonic development, plant growth, and patterning, and the *Drosophila* homolog IME4 is expressed in ovaries and testes and is essential for viability (reviewed in Niu et al., 2013).

While m⁶A has been suggested to affect almost all aspects of RNA metabolism, the molecular function of this modification remains incompletely understood (Niu et al., 2013). Importantly, m⁶A modifications are reversible in mammalian cells. Two members of the alpha-ketoglutarate-dependent dioxygenases protein family, fat-mass and obesity associated protein (FTO) and ALKBH5, have been shown to act as m⁶A demethylases (Jia et al., 2011; Zheng et al., 2013). Manipulating global m⁶A levels has implicated m⁶A modifications in a variety of cellular processes, including nuclear RNA export, control of protein translation, and splicing (reviewed in Meyer and Jaffrey, 2014). Recently, m⁶A modification has been suggested to play a role in controlling transcript stability because the YTH domain family of “reader” proteins specifically bind m⁶A sites and recruit the transcripts to RNA decay bodies (Kang et al., 2014; Wang et al., 2014a).

Whereas the DNA methylome undergoes dramatic reprogramming during early embryonic life, the developmental origins and functions of m⁶A in mammals are incompletely understood. Furthermore, the degree of evolutionary conservation of m⁶A sites is not known in ESCs. To date, the functions of m⁶A in mammalian cells have only been examined by RNAi knockdown. Depletion of METTL3 and METTL14 in human cancer cell lines led to decreased cell viability and apoptosis, leading to the interpretation that m⁶A is important for cell viability (Dominissini et al., 2012; Liu et al., 2014). A recent study reported that depletion of *Mettl3* inhibited mouse ESC (mESC) proliferation and led to ectopic differentiation (Wang et al., 2014b). Here we assess the conservation of the m⁶A methylome at the level of gene targets and function in mESCs and human ESCs (hESCs). We

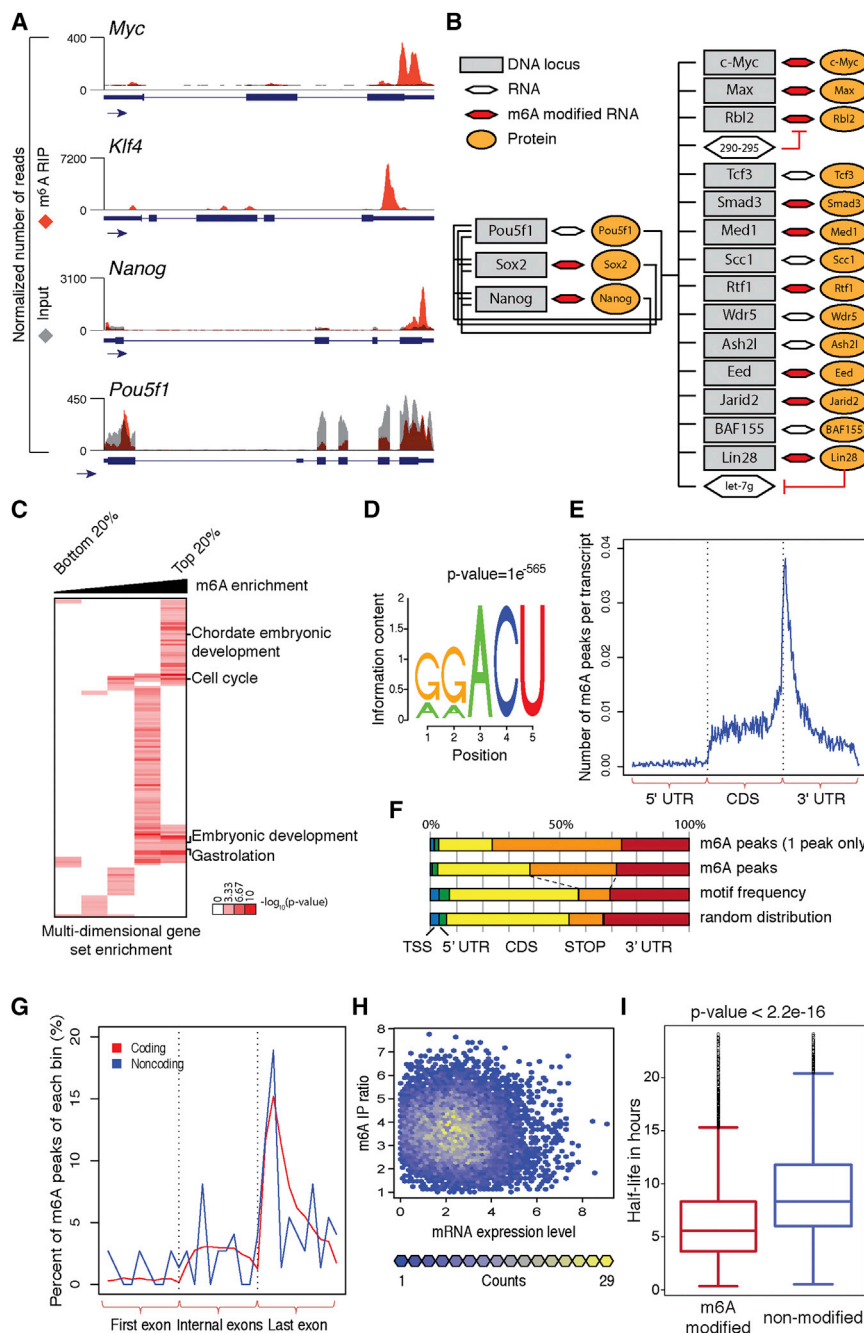


Figure 1. Topology and Characterization of m⁶A Target Genes

(A) UCSC Genome browser plots of m⁶A-seq reads along indicated mRNAs. Gray reads are from non-IP input libraries and red reads are from anti-m⁶A IP libraries. The y axis represents normalized number of reads. Blue thick boxes represent the open reading frame while the blue line represents the untranslated regions. See also Figure S1A, Table S1, and Table S2.

(B) Model of genes involved in maintenance of stem cell state (adapted from Young, 2011). Red hexagons represent modified mRNAs.

(C) Heatmap with log₁₀ (p value) of gene set enrichment analysis for m⁶A modified genes.

(D) Sequence motif identified after analysis of m⁶A enrichment regions. See also Figures S1B and S1C.

(E) Normalized distribution of m⁶A peaks across 5' UTR, CDS, and 3' UTR of mRNAs for peaks common to all samples.

(F) Graphical representation of frequency of m⁶A peaks and methylation motifs in genes, divided into five distinct regions.

(G) Distribution of m⁶A peaks across the length of mRNAs (n = 5,070) and noncoding RNAs (n = 51). See also Figures S1D–S1H.

(H) Scatter plot representation of m⁶A enrichment score (on the x axis) and gene expression level (on the y axis) for each m⁶A peak. See also Figure S1I.

(I) Box plot representing the half-life for transcripts with at least one modification site and transcripts with no modification site identified. p value calculated by Wilcoxon test. See also Figures S1J and S1K.

report the consequences of genetic ablation of *Mettl3* in mESCs as well as depletion of *METTL3* in hESCs. These experiments led to the unexpected finding that m⁶A and *METTL3* in particular are not required for ESC growth but are required for stem cells to adopt new cell fates.

RESULTS

Thousands of mESC Transcripts Bear m⁶A

To understand the role of the m⁶A RNA modification in early development, we mapped the locations of m⁶A modification across the transcriptome of mESCs and hESCs by m⁶A RNA

immunoprecipitation sequencing (RIP-seq) as described elsewhere (Dominissini et al., 2012; Meyer et al., 2012; Experimental Procedures). For each experiment, libraries were built for multiple biological replicates and concordant peaks for each experiment were used for subsequent bioinformatics analyses.

m⁶A in mRNAs of mESC Core Pluripotency Factors

We found that mRNAs encoding the core pluripotency regulators in mESCs, including *Nanog*, *Klf4*, *Myc*, *Lin28*, *Med1*, *Jarid2*, and *Eed*, were modified with m⁶A (Dunn et al., 2014; Young, 2011), whereas *Pou5f1* (also known as *Oct4*) lacked m⁶A modification (Figures 1A and 1B). We confirmed m⁶A-seq results with independent m⁶A-IP-qRT-PCR (Figure S1A available online) and m⁶A-IP followed by Nanostring nCounter analysis (m⁶A-string)

(Table S2). These validation results suggest that the m⁶A-seq data are accurate and robust. The top group of modified genes, based on degree of modification, was enriched for several functional groups, including chordate embryonic development, embryonic development, gastrulation, and cell cycle (Figure 1C). Thus, in mESCs, m⁶A targets include the ESC core pluripotency network and transcripts with dynamically controlled abundance during differentiation.

m⁶A Location and Motif in mESCs Suggest a Common Mechanism Shared with Somatic Cells

De novo motif analysis of mESC m⁶A sites specifically identified a previously described RRACU m⁶A sequence motif in somatic cells (Figures 1D and S1B) (reviewed in Meyer and Jaffrey, 2014). Furthermore, as in somatic cells, m⁶A sites in mESCs are significantly enriched near the stop codon and beginning of the 3' UTR of protein coding genes (Figures 1E and 1F), as previously described for somatic mRNAs. Although the largest fraction of m⁶A sites was within the coding sequence (CDS, 35%), the stop codon neighborhood is most enriched, comprising 33% of m⁶A sites while representing 12% of the motif occurrence. In genes with only one modification site, this bias is even more pronounced (Figure 1F). Comparison of transcript read coverage between input and wild-type (WT) revealed no bias for read accumulation around the stop codon in the input sample (Figure S1C).

In addition to the last exon, which often includes the stop codon and 3' UTR, we found a strong bias for m⁶A modification occurring in long internal exons (median exon length of 737 bp versus 124 bp; $p < 2.2 \times 10^{-16}$; two-sided Wilcoxon test), even when the number of peaks per exon was normalized for exon length or motif frequency (Figures S1D–S1F). These results suggest the possibility that processing of long exons is coupled mechanistically to m⁶A targeting through as yet unclear systems and/or that m⁶A modification itself may play a role in controlling long exon processing. The topological enrichment of m⁶A peaks surrounding stop codons in mRNAs is a poorly understood aspect of the m⁶A methylation system. We sought to understand if there was a topological enrichment or constraint on m⁶A modification in noncoding RNAs (ncRNAs), which lack stop codons. We parsed both classes of RNAs with three or more exons into three normalized bins: the first, all internal, and last exon. We observed an enrichment of m⁶A near the last exon-exon splice junction for both coding RNAs and ncRNAs and toward the 3' end of single-exon genes (Figures 1G and S1G–S1H), suggesting that the 3' enrichment of m⁶A peaks can occur independently of translation or splicing. Together, the location and sequence features we identified in mESCs suggest a mechanism for m⁶A deposition that is similar if not identical in somatic cells.

m⁶A Is a Mark for RNA Turnover

We next tested if transcript levels are correlated with the presence of m⁶A modification. Comparison of m⁶A enrichment level versus the absolute abundance of RNAs revealed no correlation between level of enrichment and gene expression (Figure 1H). A separate, quartile-based analysis found a higher percentage of m⁶A-modified transcripts in the middle quartiles of transcript abundance (Figure S1I). Thus, our analysis suggests that m⁶A

modification is not simply a random modification that occurs on abundant cellular transcripts; rather, m⁶A preferentially marks transcripts expressed at a medium level.

To further define potential mechanisms of m⁶A function, we asked whether m⁶A-marked transcripts differ from unmodified transcripts at the level of transcription, RNA decay, or translation by leveraging published genome-wide data sets in mESCs. RNA polymerase II (Pol II) occupancy at the promoters encoding both unmodified and m⁶A-marked RNAs is similar (Figure S1J). In contrast, m⁶A-marked transcripts had significantly shorter RNA half-life—2.5 hr shorter on average ($p < 2.2 \times 10^{-16}$, Figure 1I)—and increased rates of mRNA decay (average decay rate of 9 versus 5.4 for m⁶A versus unmodified, $p < 2.2 \times 10^{-16}$). m⁶A modified transcripts have slightly lower translational efficiency than unmodified transcripts (1.32 versus 1.51, respectively) (Ingolia et al., 2011) (Figure S1K). These results suggest that m⁶A is a chemical mark associated with transcript turnover.

Mettl3 Knockout Decreases m⁶A and Promotes ESC Self-Renewal

To understand the role of m⁶A methylation in ESC biology, we chose to inactivate *Mettl3*, encoding one of the components of the m⁶A methylase complex. To date no genetic study of *Mettl3* has been performed to rigorously define its requirement for m⁶A modification; all studies have relied on knockdown. We targeted *Mettl3* by CRISPR-mediated gene editing and generated several homozygous *Mettl3* knockout (KO) mESC lines. DNA sequencing confirmed homozygous stop codons that terminate translation within the first 75 amino acids, and immunoblot analysis confirmed the absence of METTL3 protein (Figures 2A and S2A). Two-dimensional thin layer chromatography (2D-TLC) showed a significant (~60%) but incomplete reduction of m⁶A in *Mettl3* KO mESC (Figures 2B and S2B). Contrary to a recent publication (Wang et al., 2014b), *Mettl3* KO slightly reduced, but did not prevent, the stable accumulation of METLL14 (Figure S2C). These experiments provide formal genetic proof that METTL3 is a major, but not the sole, m⁶A methylase in mESCs.

Contrary to the expectation in the literature, the *Mettl3* KO mESCs are viable and, surprisingly, demonstrated improved self-renewal. *Mettl3* KO mESCs could be maintained indefinitely over months and exhibited low levels of apoptosis, similar to WT mESCs, as judged by PARP cleavage and Annexin V flow cytometry (Figures 2A and S2D). We next asked whether *Mettl3* KO affected the ability of stem cells to remain pluripotent. *Mettl3* KO mESC colonies were consistently larger than WT ESCs and retained the round, compact ESC colony morphology with intense alkaline phosphatase staining, comparable to WT colonies, as well as uniform expression of NANOG and OCT4 (Figures 2C–2E and S2E and data not shown). Quantitative cell proliferation assay confirmed the increased proliferation rate of KO over WT mESCs (Figure 2F). These observations suggest that *Mettl3* KO enables enhanced mESC self-renewal. To rule out potential off-target effects from CRISPR-mediated gene targeting, we used an orthogonal approach to knock down *Mettl3* in mESCs. Two independent short hairpin RNAs (shRNAs) knocked down *Mettl3* to ~20% (Figure S2F). 2D-TLC showed an ~40% loss of m⁶A in poly(A) RNAs (Figure S2G), and apoptosis assays confirmed lack of cell death induction. Importantly, *Mettl3* depletion also increased mESC proliferation compared to control

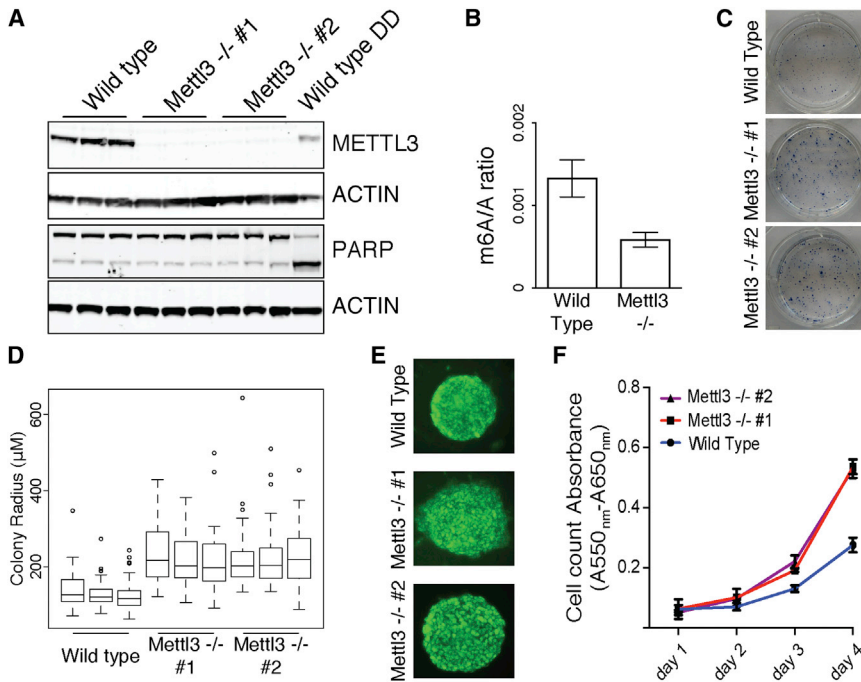


Figure 2. Characterization of Mettl3 KO Cells

(A) Western blot for METTL3 and PARP in WT and two cell lines with CRISPR-induced loss of protein (DD: DNA damaging agent). ACTIN is used as loading control. See also Figure S2A. (B) m⁶A ratio determined by 2D-TLC in WT and Mettl3 KO. Error bars represent standard deviation of three biological replicates in all panels. See also Figures S2B and S2C. (C) Alkaline phosphatase staining of WT and Mettl3 KO cells. See also Figures S2D and S2E. (D) Box plot representation of colony radius for WT and Mettl3 mutant cells. Experiments were performed in triplicate, with at least 50 colonies measured for each replicate. (E) NANOG staining of colonies of WT and two cell lines with CRISPR-induced loss of protein. (F) Cell proliferation assay of WT and two cell lines with CRISPR-induced loss of METTL3 protein. See also Figures S2F–S2H.

shRNA for one hairpin (Figure S2H). Thus, two independent approaches confirm that *Mettl3* inactivation enhanced self-renewal of ESCs.

Mettl3 KO Blocks Directed Differentiation In Vitro and Teratoma Differentiation In Vivo

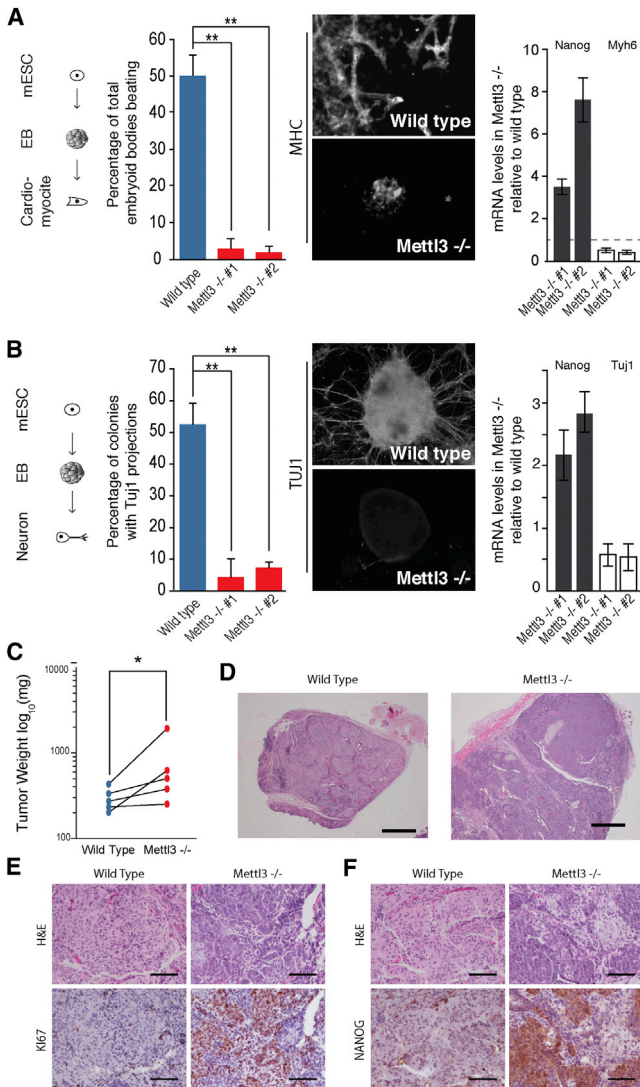
These findings, coupled with the observation that modified genes tend to have a shorter half-life, suggest that METTL3, and by extension m⁶A, is needed to fine-tune and limit the level of many ESC genes, including pluripotency regulators. Since *Mettl3* KO cells are capable of self-renewal, we tested their capacity for directed differentiation in vitro toward two lineages: cardiomyocytes (CMs) and the neural lineage. While the WT cells were able to generate beating CMs (~50% of colonies), only ~3% of *Mettl3* KO colonies of two independent clones produced beating CMs. Furthermore, differentiated colonies of *Mettl3* KO cells retained high levels of *Nanog* expression but lacked expression of the CM structural protein *Myh6*, reflecting a larger number of cells that failed to exit the mESC program in the mutant cells (Figure 3A, Movie S1, and Movie 2). Similarly, upon directed differentiation to the neural lineage, we observed a marked difference between the ability of the two cell types to differentiate. To assay for neural differentiation we stained for TUJ1, a beta-3 tubulin expressed in mature and immature neurons. While ~53% of WT colonies had TUJ1+ projections, less than 6% of *Mettl3* KO colonies had TUJ1+ projections in both KO clones (Figure 3B). Additionally, differentiated *Mettl3* KO cells showed an impaired ability to repress *Nanog* and activate *Tuj1* mRNA (Figure 3B).

To confirm the role of METTL3 in mESC differentiation in vivo, we injected *Mettl3* KO or WT cells subcutaneously into the right or left flank, respectively, of SCID/Beige mice (n = 5). Both WT and *Mettl3* KO cells formed tumors consistent in morphology with teratomas. Mutant tumors tended to be larger, in accor-

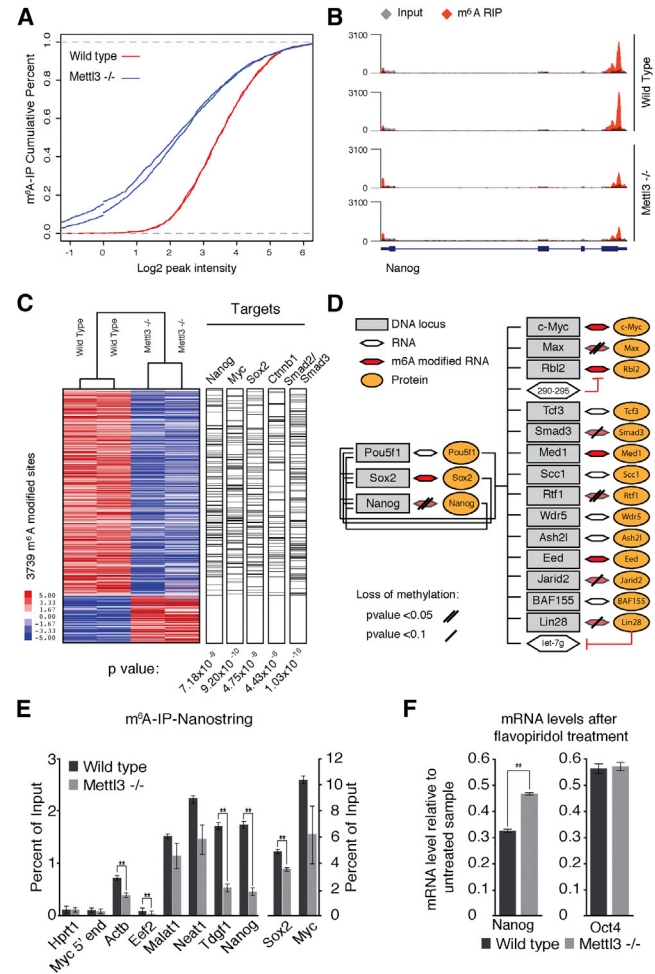
dance with mutant cell growth curves observed in vitro (Figure 3C). Histological analysis of H&E stained tumor sections revealed consistent differences between the two populations. While both groups of cells formed teratomas that contained some degree of differentiation into all three germ layers, the teratomas derived from KO cells were predominantly composed of poorly differentiated cells with very high mitotic indices and numerous apoptotic bodies, whereas WT cells differentiated predominantly into neuroectoderm (Figure 3D). Analysis of adjacent sections revealed that the mutant teratomas have markedly higher staining of the proliferation marker Ki67 and the ESC protein NANOG, which highlight the poorly differentiated cells (Figures 3E, 3F, and S3A). *Mettl3* KO tumors had higher levels of *Nanog*, *Oct4*, and *Ki67* mRNAs and lower levels of *Tuj1*, *Myh6*, and *Sox17* mRNAs (Figure S3B). These results suggest that insufficient m⁶A leads to a block in ESC differentiation and persistence of a stem-like, highly proliferative state.

Mettl3 Target Genes in mESCs

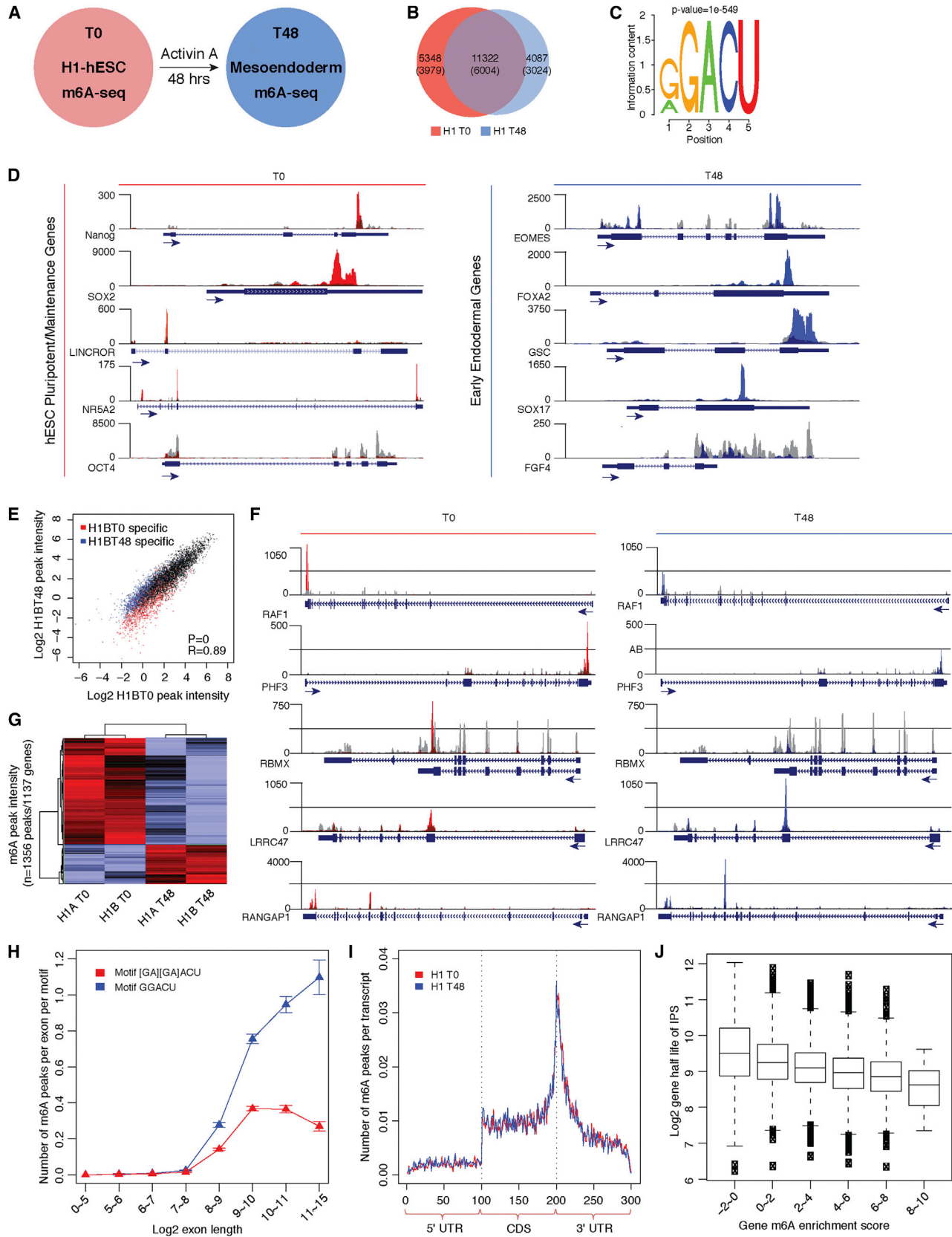
The incomplete loss of bulk m⁶A in *Mettl3* KO cells may result because METTL3 is solely responsible for the methylation of a subset of genes or sites and/or because METTL3 functions in a redundant fashion with another methylase on all m⁶A-modified genes. To distinguish between these possibilities, we mapped the m⁶A methylome in *Mettl3* KO cells. Comparison of the methylomes of WT versus *Mettl3* KO mESCs revealed a global loss of methylation across m⁶A sites identified in WT (Figure 4A). We detected changes in 3,739 sites (in 3,122 genes), including modification sites in *Nanog* mRNA. Thus, this unbiased analysis suggested a set of targets that rely more exclusively on METTL3, including *Nanog* and other pluripotency mRNAs (Figures 4B and 4C) (Table S1). Gene set enrichment analysis confirmed that METTL3-target genes significantly overlap functional gene sets important for pluripotency, including targets of CTNNB1 (4.43 × 10⁻⁶), targets of SMAD2 or SMAD3 (1.03 × 10⁻¹⁶), targets of MYC (9.20 × 10⁻¹⁰), targets of



SOX2 (4.75×10^{-8}), and targets of NANOG (7.18×10^{-8}) ([Figure 4C](#)), and include 5 of 11 core ESC regulators such as *Nanog*, *Rlf1*, *Jarid2*, and *Lin28* ([Figure 4D](#)). Independent validation by



m⁶A RIP followed by Nanostring detection confirmed loss of m⁶A in *Nanog* and other mRNAs in KO versus WT mESCs ([Figure 4E](#)). Further, after transcription arrest by flavopiridol treatment, *Nanog* mRNA showed delayed turnover in *Mett13* KO cells compared to WT, consistent with a requirement for m⁶A in *Nanog* mRNA turnover ([Figure 4F](#)). However, RNA-seq analysis of *Mett13* KO cells revealed modest perturbations in mRNA steady state levels with only ~300 genes demonstrating



(legend on next page)

significant changes over 1.5-fold. Collectively, these results suggest that ESC genes are under METTL3 control and that m⁶A impacts ESC biology.

Widespread m⁶A Modification of hESCs

The identification of thousands of m⁶A sites raises the challenge of defining the functional importance of each and every one of the sites. We reasoned that evolutionary conservation provides a powerful and comprehensive metric of function. To this end, we mapped m⁶A sites in hESCs and during endoderm differentiation to elucidate the patterns and potential conservation of m⁶A methylome (Figure 5A). In basal state hESCs [Time (T) = 0], m⁶A-seq identified 16,943 peaks in 7,871 genes representing 7,530 coding and 341 noncoding RNAs. Upon hESC differentiation toward endoderm (T = 48, “endoderm differentiation” thereafter), m⁶A-seq identified 15,613 m⁶A peaks in 7,195 genes representing 6,909 coding and 286 noncoding RNAs (Table S3). As shown in Figure 5B, 11,322 peaks (6,004 genes) were common between the undifferentiated and differentiated hESCs, while 5,348 (3,979 genes) versus 4,087 peaks (3,024 genes) were unique, respectively.

Many Master Regulators of hESC Maintenance and Differentiation Are Modified with m⁶A

As we observed for mESC, transcripts encoding many hESC master regulators, including human *NANOG*, *SOX2*, and *NR5A2*, were m⁶A modified. As in mESCs, the transcripts for *OCT4* (*POU5F1*) in hESCs did not harbor an m⁶A modification (Figure 5D). These results show that in both organisms the core pluripotency/maintenance genes are under the regulatory influence of the m⁶A pathway. We also identified human-specific lncRNAs with known roles in hESC maintenance, such as *LINC-ROR* and *MEGAMIND/TUNA*, to contain m⁶A modifications (Figures 5D and S4A) (Lin et al., 2014; Loewer et al., 2010). Upon induction of hESC differentiation, we observed transcripts encoded by several key regulators of endodermal differentiation, including *EOMES* and *FOXA2* (Figure 5D), to also have m⁶A modifications. Gene ontology (GO) analyses of methylated genes in undifferentiated hESCs, and after endodermal differentiation, were significantly enriched in biological functions such as regulation of transcription (FDR = 1.2×10^{-14}), chordate embryonic

development (FDR = 1.1×10^{-4}), and regulation of cell morphogenesis (FDR = 0.01).

Upon hESC differentiation toward endoderm, 1,356 peaks in 1,137 genes showed quantitative differences of at least 1.5-fold in m⁶A intensity, after normalization for input transcript abundance (Figures 5E and 5F and Table S4). The majority of these differential m⁶A sites represented quantitative differences at existing sites (i.e., 59.1% of the peaks were called in both time points), rather than state-specific de novo appearance or erasure of modification (Figure 5G). This is consistent with the observation that 74.9% of sites in the hESCs overlapped those observed in HEK293T data (Meyer et al., 2012) and the minimal changes in m⁶A sites observed in a recent survey of m⁶A pattern across cell types (Schwartz et al., 2014). We suggest that transcripts exhibit dynamic differential peak m⁶A methylation intensity largely at “hard-wired sites” during differentiation under the conditions examined and when compared to other tissue types.

Conserved Features of m⁶A Modifications Spanning Different Species

We found that three salient features of the m⁶A methylome are conserved in hESCs. First, m⁶A sites in hESCs are also dominated by the RRACU motif seen in mESC and somatic cells (Dominissini et al., 2012; Meyer et al., 2012) (Figure 5C). There was also a strong preference for the methylome to target long-internal exons at the RRACU motif even after we normalized for exon length and number of m⁶A motifs (Figure 5H). Second, there was a significant enrichment in m⁶A peaks at the 3' end of transcripts, near the stop codon of coding genes or the last exon in noncoding RNAs (Figures 5I and S4B–S4D). Furthermore, the topology of m⁶A modification is preserved upon endodermal differentiation (Figure 5I). As in mESCs, moderately to lowly expressed genes have higher probabilities of becoming methylated (Figure S4E). Lastly, hESC m⁶A is not correlated with transcription rate as judged by Global Run-On sequencing (GRO-seq) (Sigova et al., 2013), but it is strongly anticorrelated with measured mRNA half-life in human pluripotent cells (Neff et al., 2012), strongly suggesting that m⁶A modification also marks RNA turnover in hESCs (Figures 5J, S4F, and S4G).

Figure 5. m⁶A-seq Profiling of hESCs during Endoderm Differentiation

- (A) m⁶A-seq was performed in resting (undifferentiated) human H1-ESCs (T0) and after 48 hrs of Activin A induction toward endoderm (mesoendoderm) (T48).
(B) Venn diagram of the overlap between high-confidence T0 and T48 m⁶A peaks. The number of genes in each category is shown in parenthesis. See also Table S3 and Table S4.
(C) Sequence motif identified after analysis of m⁶A enrichment regions.
(D) UCSC Genome browser plots of m⁶A-seq reads along indicated RNAs. Gray reads are from non-IP control input libraries and red (T0) or blue (T48) reads are from anti-m⁶A IP libraries. y axis represents normalized number of reads; x axis is genomic coordinates. Key regulators of stem cell maintenance (left) and master regulators of endoderm differentiation (right) are represented. See also Figure S4A.
(E) Scatter plot of m⁶A peak intensities between two different time points (T0 versus T48) of the same biological replicate with only “high-confidence” T0 or T48 specific peaks supported by both biological replicates highlighted.
(F) UCSC Genome browser plots of m⁶A-seq reads along indicated mRNAs in undifferentiated (T0) versus differentiated (T48) cells. The gray reads are from non-IP control input libraries. The red and blue reads are from the anti-m⁶A RIP of T = 0 and T = 48 samples, respectively.
(G) Differential intensities of m⁶A peaks (DMPs) identify hESC cell states T0 versus T48 hrs. Z score scaled log₂ peak intensities of DMPs are color-coded according to the legend. The peaks and samples are both clustered by average linkage hierarchical clustering using 1-Pearson correlation coefficient of log₂ peak intensity as the distance metric.
(H) Number of peaks per exon normalized by the number of motifs (on sense strand) in the exon. The error bars represent standard deviations from 1,000 times of bootstrapping.
(I) The normalized distribution of m⁶A peaks across the 5' UTR, CDS, and 3' UTR of mRNAs for T0 and T48 m⁶A peaks. See also Figures S4B–S4D.
(J) Box plot representing the half-life for transcripts, with transcripts separated according to enrichment score. See also Figures S4E, S4F, and S4G.

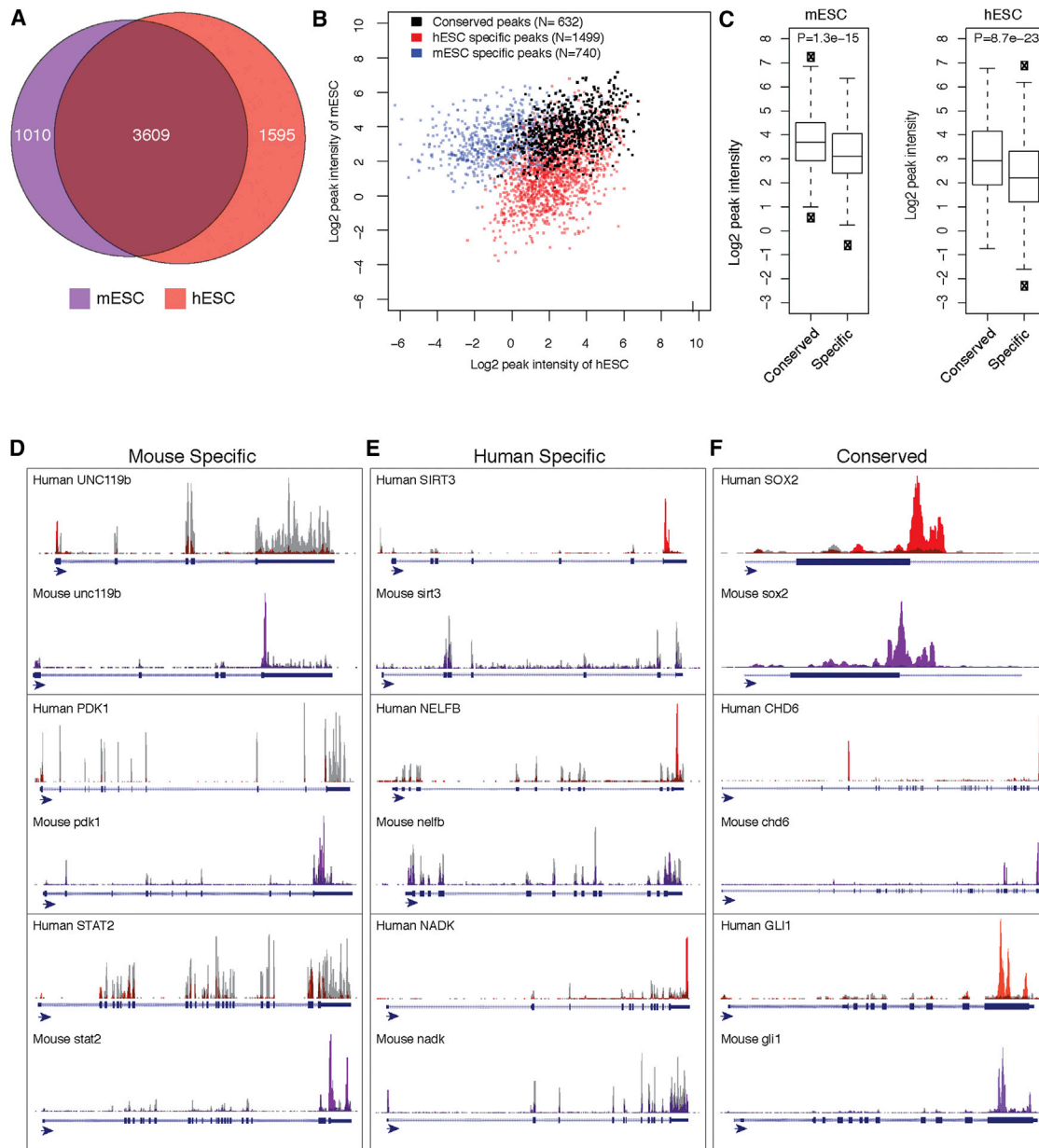


Figure 6. Evolutionary Conservation and Divergence of the m⁶A Epi-transcriptomes of hESCs and mESCs

(A) Venn diagram showing a 62% overlap between methylated genes in *Mus musculus* (purple) and *Homo sapiens* (red) ESCs ($p = 3.5 \times 10^{-92}$; Fisher exact test). See also Table S5 and Table S6.

(B) The m⁶A peaks that could be mapped to orthologous genomic windows between mouse and human were identified. The intensities of m⁶A-seq signals in hESCs and mESCs were shown for m⁶A peaks found to be unique in mouse (blue), unique in human (red), and conserved between human and mouse (black). (C) Box plot of peak intensities of m⁶A sites conserved (“common”) or not conserved (“specific”) in mESCs and hESCs. ($p = 1.3 \times 10^{-15}$ and 8.7×10^{-23} , respectively, Wilcoxon test).

(D–F) UCSC Genome browser plots of m⁶A-seq reads along indicated mRNAs. The gray reads are from non-IP control input libraries and the purple and red reads are from the anti-m⁶A RIP of mESCs and hESCs (T0), respectively. (D) Mouse-specific m⁶A modifications are represented. (E) Human-specific m⁶A modifications of ESCs are represented. (F) Conserved m⁶A modifications at the gene and site level are represented. Genes such as *CHD6* have a conserved m⁶A peak location at its 3' UTR as well as mouse- and human-specific m⁶A peaks at conserved but distinct exons.

Evolutionary Conservation and Divergence of the m⁶A Epi-transcriptomes of Human and Mouse ESCs

Previous studies suggested significant conservation of m⁶A modified genes between mouse and human in somatic cell types, but the comparisons are limited by nonmatched tissue types

(Dominissini et al., 2012; Meyer et al., 2012). We were thus interested in examining the evolutionary conservation of hESC and mESC m⁶A methylomes. At the gene level, 69.4% (3,609 of 5,204) of hESC genes are also m⁶A modified in the orthologous mouse gene ($p = 8.3 \times 10^{-179}$, Fisher exact test) (Figure 6A;

Table S5). Furthermore, we identified 632 conserved m⁶A peak sites (46.1%) between hESCs and mESCs (Table S6). Notably, conserved sites tend to have higher m⁶A peak intensities compared to m⁶A peak sites that were not conserved (Figures 6B and 6C, $p = 1.3 \times 10^{-15}$ and 8.7×10^{-23} for hESCs or mESCs, respectively; Wilcoxon test). Commonly methylated genes can demonstrate m⁶A modification sites at identical sites (as in the case of *GLI1*), similar but not identical locations (as in the case of *SOX2*), or m⁶A sites at different exons (as in the case of *CHD6*) (Figures 6D–6F and Table S4). Our data thus reveal a substantial overlap at the gene level, suggesting broad functional significance of m⁶A modification in ESCs in both species. At the same time, we also observed numerous species-specific m⁶A patterns that may contribute to specific aspects of ESC biology (Schnerch et al., 2010).

METTL3 Is Required for hESC Differentiation

To address the function of m⁶A in hESCs, we generated hESC colonies with stable knockdown of *METTL3* and shRNA control (Figure 7A). Knockdown of *METTL3* in hESCs resulted in reduction in *METTL3* mRNA levels and reduction in m⁶A level (Figures 7B and 7C and Figures S5B and S5C). *METTL3*-depleted hESCs could be stably maintained, suggesting the dispensability of *METTL3* for hESC self-renewal or viability. Strikingly, differentiation of *METTL3*-depleted hESCs into neural stem cells (NSCs) by dual inhibition of SMAD signaling, using Dorsomorphin and SB-431542, revealed a block in neuronal differentiation (Experimental Procedures). While 44% ($\pm 3.5\%$ SD) of the control cells were SOX1+, only 10% ($\pm 3.1\%$ SD) of the *METTL3*-depleted were SOX+ (Figure S5A).

Similarly, knockdown of *METTL3*, in three independently generated hESC colony clones selected for *METTL3* knockdown, led to a profound block in endodermal differentiation at day 2 and day 4 based on their failure to express the endoderm markers *EOMES* and *FOXA2* compared to either two shRNA control colony clones (Figure 7D) or WT hESCs (Figure S5D). Consistently, *METTL3*-depleted ESCs retain high levels of expression of the master regulators *NANOG* and *SOX2* throughout the differentiation time course in contrast to their diminishing expression in WT cells (Figures 7E and S5E). These results indicate that *METTL3* and m⁶A control differentiation of hESCs.

DISCUSSION

m⁶A Methylome in ESCs

Our analysis of the ESC m⁶A methylome in mouse and human cells reveals extensive m⁶A modification of ESC genes, including most key regulators of ESC pluripotency and lineage control. However, this observation does not mean that m⁶A is uniquely tied to the pluripotency network. Because m⁶A marks moderately expressed transcripts that need to be turned over in a timely fashion, such genes in ESCs likely include many regulators of pluripotency and lineage determination. The pattern and sequence motif associated with ESC m⁶A are similar if not identical to those previously reported in somatic cells, suggesting a single mechanism that deposits m⁶A modification in early embryonic life. This invariant mechanism for m⁶A contrasts with the complexity of 5-methyl-cytosine in DNA and histone

lysine methylations that undergo extensive reprogramming with distinct rules in pluripotent versus somatic cells.

We identified a general and conserved topological enrichment of m⁶A sites at the 3' end of genes among single-exon and multiple-exon mRNAs as well as ncRNAs. Thus, neither the stop codon nor the last exon-exon splice junction can alone explain the observed m⁶A topology in RNA. However, all species examined to date including *Saccharomyces cerevisiae* and *A. thaliana* exhibit a strong 3' bias in m⁶A localization, suggesting an evolutionary constraint that may target the m⁶A modification to the 3' ends of genes regardless of gene structure or coding potential. This bias may be achieved by preferential m⁶A methylase recruitment to 3' sites or preferential action of demethylases in upstream regions of the transcript. Although the role of demethylases cannot be excluded, the observation of 3' end m⁶A bias in *S. cerevisiae*, which lacks known m⁶A demethylases, argues against the latter mechanism (Bodi et al., 2012; Jia et al., 2011; Schwartz et al., 2013; Zheng et al., 2013). The functional importance of m⁶A location versus its specific molecular outcome needs to be addressed in future studies.

Mettl3 Selectively Targets mRNAs, Including Pluripotency Regulators

While several studies had approached *Mettl3* function by RNAi knockdown (Dominissini et al., 2012; Fustin et al., 2013; Liu et al., 2014; Wang et al., 2014b), genetic ablation of *Mettl3* allowed us to examine the true loss-of-function phenotypes. The importance of using definitive genetic models is highlighted by recent studies in the DNA methylation field where shRNA experiments led to misassigned functions of Ten-eleven translocation (TET) proteins that were later recognized in genetic KOs (Dawlaty et al., 2011, 2013). We found that both *Mettl3* KO and depletion led to incomplete reduction of the global levels of m⁶A in both mESCs and hESCs, demonstrating redundancy in m⁶A methylases. However, m⁶A profiling in *Mettl3* KO cells revealed a subset of targets, approximately 33% of m⁶A peaks, that are preferentially dependent on *METTL3*, and these included *Nanog*, *Sox2*, and additional pluripotency genes. A second m⁶A methylase, *METTL14*, was described during the preparation of this manuscript.

RNAi knockdown of *METTL3* in somatic cancer cells led to apoptosis (Dominissini et al., 2012), and one study reported ectopic differentiation of mESCs with *Mettl3* depletion (Wang et al., 2014b). In contrast, we found that *Mettl3* KO does not affect mESC cell viability or self-renewal, and in fact mESCs renewed at an improved rate. The differences in phenotype observed could potentially be explained by different dependency on m⁶A modified RNAs in different cell types, acute versus chronic inactivation, or RNAi off-target effects. m⁶A methylome analysis in different cell types with *Mettl3* inactivation may shed light on these differences in the future.

Conservation of m⁶A Methylome in Mammalian ESCs

The conserved methylation patterns of many ESC master regulators and the shared phenotype observed upon inactivation of *Mettl3* suggest that *METTL3* operates to control stem cell differentiation. It is known that hESCs and mESCs are not equivalent (Schnerch et al., 2010) and are cultured in different conditions. By focusing in on orthologous genes, we were able to

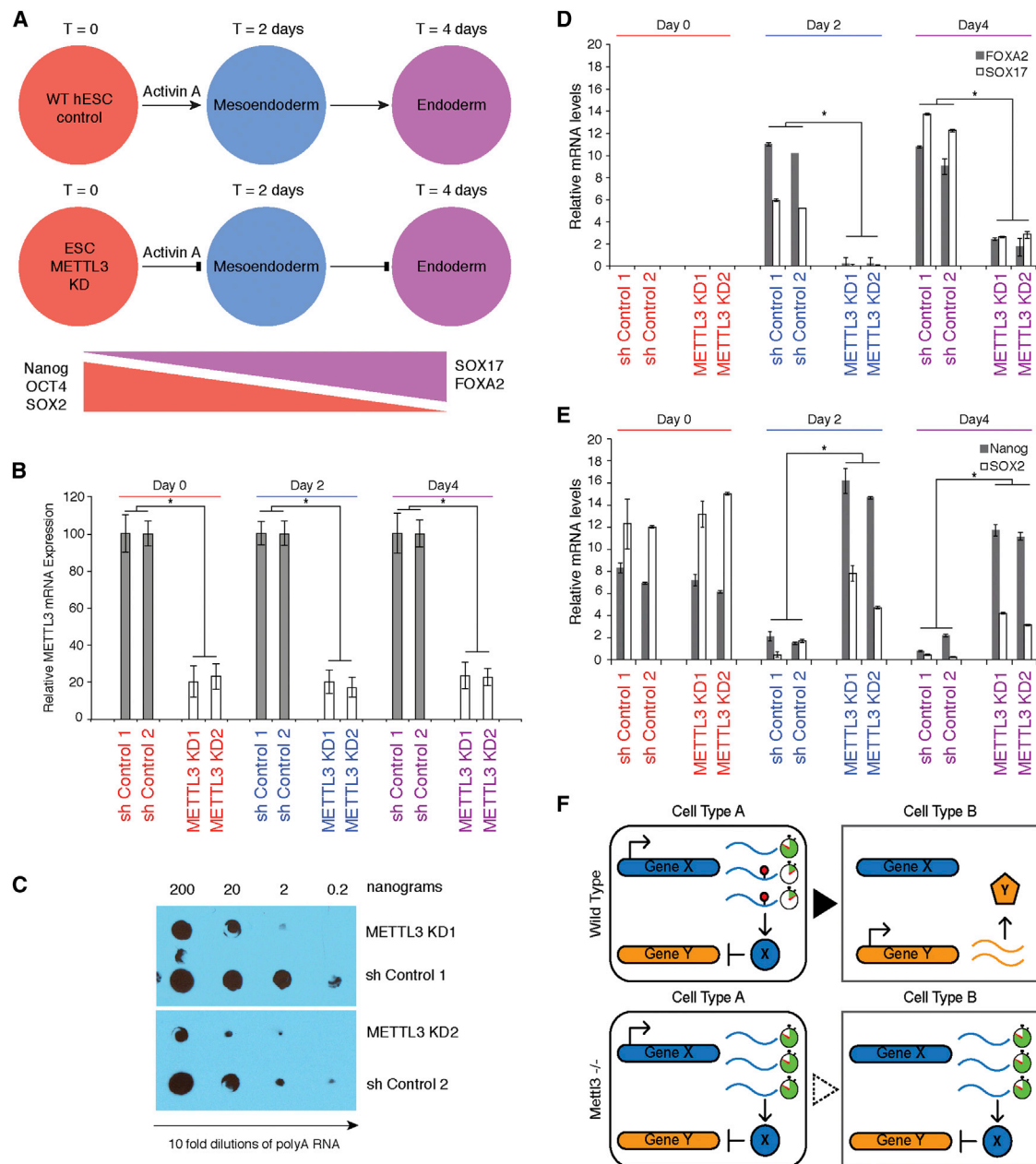


Figure 7. METTL3 Is Required for Normal hESC Endoderm Differentiation: A Model of METTL3 Function

(A) hESC cells were transfected with anti-METTL3 shRNA (KD) as well as control shRNA and stable hESC colonies were obtained after drug selection. Two independent clones were subjected to endodermal differentiation with Activin A and examined at various indicated time points. A schematic of the trends of gene expression for indicated markers of stem maintenance and endoderm differentiation is also shown. See also Figure S5A.

(B) Levels of *METTL3* mRNA in hESC cells with control shRNA versus anti-METTL3 shRNA (KD) across the three indicated time points during endodermal differentiation ($n = 2$ independent generated ESC knockdown and control clones shown). In all panels, error bars represent standard deviation across three replicates per time point; * $p < 0.05$ t test (two-tailed) between different clones. See also Figure S5B.

(C) Anti-m⁶A dot-blot was performed on 10 \times fold dilutions of poly(A)-selected RNA from hESCs derived from control shRNA versus anti-METTL3 shRNA clones. See also Figure S5C.

(D and E) mRNA levels of endodermal and stem maintenance/marker genes. qRT-PCR was performed on indicated genes and time points ($n = 2$ independently generated ESC knockdown and control clones shown). See also Figure S5D.

(F) Model: m⁶A marks transcripts for faster turnover. Upon transition to new cell fate, m⁶A marked transcripts are readily removed to allow the expression of new gene expression networks. In the absence of m⁶A, the unwanted presence of transcripts will disturb the proper balance required for cell fate transitions.

catalog both shared and species-specific methylation sites. The observation that certain methylation sites are modified whenever a target transcript is expressed in both species, despite cell state or culture differences, argues that these modification events have been preserved under strong purifying selection during evolution. Our comparative genomic analyses also pave the way to further understand potential biological differences between hESCs and mESCs at the level of m⁶A epi-transcriptome, given the unique patterns of some methylation sites between the species.

RNA “Antiepigenerics:” m⁶A as a Mark of Transcriptome Flexibility

Stem cell gene expression programs need to balance fidelity and flexibility. On the one hand, stem cell genes need sufficient stability to maintain self-renewal and pluripotency over multiple cell generations, but on the other hand, gene expression needs to change dynamically and rapidly in response to differentiation cues. It has been proposed that ESC gene expression programs are in constant flux between competing fates, and pluripotency is a statistical average (Loh and Lim, 2011; Montserrat et al., 2013; Shu et al., 2013). We found that mRNAs with m⁶A tend to have a shorter half-life, and *Nanog* and *Sox2* mRNAs could not be properly downregulated with differentiation in METTL3-deficient mESCs and hESCs. However, METTL3 deficiency has only modest effects on steady state gene expression, which could arise from the nonstoichiometric nature of the m⁶A modification. The application of methods that can determine the level of modification of each RNA species will allow us to answer these questions (Harcourt et al., 2013; Liu et al., 2013). *Mettl3* KO mESCs have enhanced self-renewal but hindered differentiation, concomitant with a decreased ability to downregulate ESC mRNAs. WTAP, a conserved METTL3 interacting partner from yeast to human cells (Horiuchi et al., 2013; Schwartz et al., 2014), is also required for endodermal and mesodermal differentiation (Fukusumi et al., 2008). The observed phenotypes in ESCs and teratomas are all the more notable because we have significantly reduced, but not eliminated, m⁶A.

Our findings suggest a model where m⁶A serves as the necessary flexibility factor to counterbalance epigenetic fidelity—an RNA “antiepigenerics” measure (Figure 7F). m⁶A marks a wide range of transcripts, including ESC fate determinants to limit their level of expression and ensure their continual degradation so that cells can rapidly transition between gene expression programs. In ESCs, m⁶A is required for cells to rapidly exit the pluripotent state upon differentiation. The inability to exit the stem cell state and continued proliferation upon insufficient m⁶A offers a potential explanation for the association of FTO with human cancers (Loos and Yeo, 2014). METTL3 depletion also leads to elongation of the circadian clock (Fustin et al., 2013), suggesting a role for m⁶A in resetting the transcriptome. In yeast, m⁶A is active during meiosis (Clancy et al., 2002), where diploid gene expression programs are reset to generate haploid offspring. We propose that m⁶A makes the transition between cell states possible by facilitating a reset mechanism between stages, as occurs in ESCs and likely other cell types. In contrast to epigenetic mechanisms that provide cellular memory of gene expression states, m⁶A enforces the transience of genetic information, helping cells to forget the past and thereby embrace the future.

EXPERIMENTAL PROCEDURES

For full details, see the [Supplemental Experimental Procedures](#).

Mouse Cell Culture and Differentiation

J-1 murine ESCs were grown under typical feeder-free ESC culture conditions. For CM formation, mESCs were differentiated in CM differentiation media and scored on day 12. For neuron formation, mESCs were differentiated in MEF and ITSFn medium and scored after 10 days in ITSFn medium. For the cell proliferation assay 5,000 cells were cultured in 24-well plates and the assay was performed according to the manufacturer’s protocol (MTT assay, Roche). For the single-colony assays and Nanog staining, 1,000 cells were cultured per well, on a six-well plate. For alkaline phosphatase staining, cells were stained according to the manufacturer’s protocol (Vector Blue Alkaline Phosphatase Substrate Kit).

hESC Cell Culture, Transfection, and Differentiation

H1 (WA01) cells were cultured in feeder-free conditions as described elsewhere (Sigova et al., 2013). Stable hESC lines were created that expressed shMETTL3 RNA or scrambled shRNA by transfection of hESCs with plasmids encoding shMETTL3 or scrambled shRNA and a puromycin resistance gene. Cells were treated with puromycin for 6 days beginning 2 days after transfection. For scrambled shRNA and METTL3 shRNA, two and three independent puromycin-resistant colonies were picked and expanded, respectively. Endodermal differentiation was then induced by Activin A, as described elsewhere (Sigova et al., 2013). Day 2 and Day 4 of differentiation were measured from the time that Activin A was added. Puromycin was removed from the media 1 day prior to endodermal differentiation.

RNA m⁶A-IP and m⁶A Methylation IP RNA-Seq Analysis

Libraries generated with iCLIP adaptors were separated by barcode, and perfectly matching reads were collapsed. Sequencing reads were mapped using TopHat (Trapnell et al., 2009). A nonredundant mm9 transcriptome was assembled from UCSC RefSeq genes, UCSC genes, and predictions from Ulitsky et al. (2011) and Guttman et al. (2011). For human data sets, the Ensembl genes (release 64) were used. We performed the search for enriched peaks by scanning each gene using 100-nucleotide sliding windows and calculating an enrichment score for each sliding window (Dominissini et al., 2012). HOMER software package (Heinz et al., 2010) was used for de novo discovery of the methylation motif.

CRISPR-Mediated *Mettl3* KO

Plasmids for guide RNA (design with CRISPR design tool; Hsu et al., 2013), a human codon optimized Cas9 expression plasmid, and a plasmid with a puromycin resistance cassette were cotransfected. Cells were plated at low density for single-colony isolation and selected single colonies were tested by western blot for loss of protein.

Determination of m⁶A Levels

2D-TLC was performed as described by Jia et al. (2011). For dot-blots, the indicated amounts of RNA were applied to the membrane and cross-linked by UV. The m⁶A primary antibody was added at a concentration of 1:500. The membrane was incubated with the secondary antibody and exposed to an autoradiographic film. m⁶A RNA mass-spectrometry was performed as described in the [Supplemental Experimental Procedures](#).

Data Set Comparison

Mouse Pol II occupancy data, mRNA half-life, and protein translation efficiency were obtained from Rahi et al. (2010), Sharova et al. (2009) and Ingolia et al. (2011). Plotting and statistical tests were performed in R. Multidimensional gene set enrichment analysis over DAVID GO terms and stem cell gene sets (Wong et al., 2008) were performed using Genomica (Segal et al., 2003).

Teratoma Generation and Histopathology

WT and *Mettl3* mutant cells were subcutaneously injected into 8-week-old female SCID/Beige mice (Charles River). Four weeks after injection, the mice were euthanized and the tumors were harvested. All animal studies were approved by Stanford University IACUC guidelines. For histological

analysis, slides were stained with hematoxylin and eosin (H&E) or stained by immunohistochemistry (IHC) with VECTASTAIN ABC Kit and DAB Peroxidase Substrate Kit following the manufacturer's instructions. Analyses were performed by a boarded veterinary pathologist (D.M.B.).

ACCESSION NUMBERS

The accession numbers for the RNA sequencing data are GSE52681 (mouse) and GSE52600 (human).

SUPPLEMENTAL INFORMATION

Supplemental Information for this article includes five figures, Supplemental Experimental Procedures, six tables, and two movies and can be found with this article online at <http://dx.doi.org/10.1016/j.stem.2014.09.019>.

AUTHOR CONTRIBUTIONS

P.J.B. and H.Y.C. conceived of the mESC studies; P.J.B., L.L., D.M.B., E.L., A.C.C., R.A.F., M.W., Y.X., and H.Y.C. designed and performed experiments in the mouse system. A.C.M., Y.X., and C.C.G. conceived of the hESC studies; B.M., B.H., K.D., C.Z., K.L., P.D., M.W., A.C.M., Y.X., and C.C.G. designed and performed experiments in the human system. J.W., K.Q., and J.Z. analyzed the data. P.J.B., B.M., J.W., Y.X., C.C.G., and H.Y.C. wrote the paper with input from all authors.

ACKNOWLEDGMENTS

We thank C. He, C. Mason, S. Schwartz, A. Regev, J.M. Claycomb, N. Van Witenbergh, B.D. Howard, and members of the Chang and Giallourakis labs for discussions and assistance. We thank H.E. Arda and S.K. Kim for help with FACS analysis and A. Memmelaar for his expertise in graphic arts. This work was supported by the California Institute for Regenerative Medicine and NIH R01-CA118750 (H.Y.C.), the MGH Start-Up Funds and MGH ECOR grant 2013A051178 (C.C.G.), NIH grant DK090122 (A.C.M.), and the Eli and Edythe Broad Center of Regenerative Medicine and Stem Cell Research at UCLA Research Award (Y.X.). P.J.B. is the Kenneth G. and Elaine A. Langone Fellow of the Damon Runyon Cancer Research Foundation. Y.X. is an Alfred Sloan Foundation Research Fellow. H.Y.C. is an Early Career Scientist of the Howard Hughes Medical Institute.

Received: April 3, 2014
Revised: August 14, 2014
Accepted: September 30, 2014
Published: October 16, 2014

REFERENCES

Bodi, Z., Zhong, S., Mehra, S., Song, J., Graham, N., Li, H., May, S., and Fray, R.G. (2012). Adenosine Methylation in Arabidopsis mRNA is Associated with the 3' End and Reduced Levels Cause Developmental Defects. *Front Plant Sci.* 3, 48.

Clancy, M.J., Shambaugh, M.E., Tipton, C.S., and Bokar, J.A. (2002). Induction of sporulation in *Saccharomyces cerevisiae* leads to the formation of N6-methyladenosine in mRNA: a potential mechanism for the activity of the IME4 gene. *Nucleic Acids Res.* 30, 4509–4518.

Dawlaty, M.M., Ganz, K., Powell, B.E., Hu, Y.C., Markoulaki, S., Cheng, A.W., Gao, Q., Kim, J., Choi, S.W., Page, D.C., and Jaenisch, R. (2011). Tet1 is dispensable for maintaining pluripotency and its loss is compatible with embryonic and postnatal development. *Cell Stem Cell* 9, 166–175.

Dawlaty, M.M., Breiling, A., Le, T., Raddatz, G., Barrasa, M.I., Cheng, A.W., Gao, Q., Powell, B.E., Li, Z., Xu, M., et al. (2013). Combined deficiency of Tet1 and Tet2 causes epigenetic abnormalities but is compatible with postnatal development. *Dev. Cell* 24, 310–323.

Dominissini, D., Moshitch-Moshkovitz, S., Schwartz, S., Salmon-Divon, M., Ungar, L., Osenberg, S., Cesarkas, K., Jacob-Hirsch, J., Amariglio, N.,

Kupiec, M., et al. (2012). Topology of the human and mouse m6A RNA methylomes revealed by m6A-seq. *Nature* 485, 201–206.

Dunn, S.J., Martello, G., Yordanov, B., Emmott, S., and Smith, A.G. (2014). Defining an essential transcription factor program for naïve pluripotency. *Science* 344, 1156–1160.

Fu, Y., and He, C. (2012). Nucleic acid modifications with epigenetic significance. *Curr. Opin. Chem. Biol.* 16, 516–524.

Fukusumi, Y., Naruse, C., and Asano, M. (2008). Wtap is required for differentiation of endoderm and mesoderm in the mouse embryo. *Dev. Dyn.* 237, 618–629.

Fustin, J.M., Doi, M., Yamaguchi, Y., Hida, H., Nishimura, S., Yoshida, M., Isagawa, T., Morioka, M.S., Takeya, H., Manabe, I., and Okamura, H. (2013). RNA-methylation-dependent RNA processing controls the speed of the circadian clock. *Cell* 155, 793–806.

Guttman, M., Donaghey, J., Carey, B.W., Garber, M., Grenier, J.K., Munson, G., Young, G., Lucas, A.B., Ach, R., Bruhn, L., et al. (2011). lincRNAs act in the circuitry controlling pluripotency and differentiation. *Nature* 477, 295–300.

Harcourt, E.M., Ehrenschrwender, T., Batista, P.J., Chang, H.Y., and Kool, E.T. (2013). Identification of a selective polymerase enables detection of N(6)-methyladenosine in RNA. *J. Am. Chem. Soc.* 135, 19079–19082.

Heinz, S., Benner, C., Spann, N., Bertolino, E., Lin, Y.C., Laslo, P., Cheng, J.X., Murre, C., Singh, H., and Glass, C.K. (2010). Simple combinations of lineage-determining transcription factors prime cis-regulatory elements required for macrophage and B cell identities. *Mol. Cell* 38, 576–589.

Horiuchi, K., Kawamura, T., Iwanari, H., Ohashi, R., Naito, M., Kodama, T., and Hamakubo, T. (2013). Identification of Wilms' tumor 1-associating protein complex and its role in alternative splicing and the cell cycle. *J. Biol. Chem.* 288, 33292–33302.

Hsu, P.D., Scott, D.A., Weinstein, J.A., Ran, F.A., Konermann, S., Agarwala, V., Li, Y., Fine, E.J., Wu, X., Shalem, O., et al. (2013). DNA targeting specificity of RNA-guided Cas9 nucleases. *Nat. Biotechnol.* 31, 827–832.

Ingolia, N.T., Lareau, L.F., and Weissman, J.S. (2011). Ribosome profiling of mouse embryonic stem cells reveals the complexity and dynamics of mammalian proteomes. *Cell* 147, 789–802.

Jia, G., Fu, Y., Zhao, X., Dai, Q., Zheng, G., Yang, Y., Yi, C., Lindahl, T., Pan, T., Yang, Y.G., and He, C. (2011). N6-methyladenosine in nuclear RNA is a major substrate of the obesity-associated FTO. *Nat. Chem. Biol.* 7, 885–887.

Kang, H.J., Jeong, S.J., Kim, K.N., Baek, I.J., Chang, M., Kang, C.M., Park, Y.S., and Yun, C.W. (2014). A novel protein, Pho92, has a conserved YTH domain and regulates phosphate metabolism by decreasing the mRNA stability of PHO4 in *Saccharomyces cerevisiae*. *Biochem. J.* 457, 391–400.

Lin, N., Chang, K.Y., Li, Z., Gates, K., Rana, Z.A., Dang, J., Zhang, D., Han, T., Yang, C.S., Cunningham, T.J., et al. (2014). An evolutionarily conserved long noncoding RNA TUNA controls pluripotency and neural lineage commitment. *Mol. Cell* 53, 1005–1019.

Liu, N., Parisien, M., Dai, Q., Zheng, G., He, C., and Pan, T. (2013). Probing N6-methyladenosine RNA modification status at single nucleotide resolution in mRNA and long noncoding RNA. *RNA* 19, 1848–1856.

Liu, J., Yue, Y., Han, D., Wang, X., Fu, Y., Zhang, L., Jia, G., Yu, M., Lu, Z., Deng, X., et al. (2014). A METTL3-METTL14 complex mediates mammalian nuclear RNA N6-adenosine methylation. *Nat. Chem. Biol.* 10, 93–95.

Loewer, S., Cabili, M.N., Guttman, M., Loh, Y.H., Thomas, K., Park, I.H., Garber, M., Curran, M., Onder, T., Agarwal, S., et al. (2010). Large intergenic non-coding RNA-RoR modulates reprogramming of human induced pluripotent stem cells. *Nat. Genet.* 42, 1113–1117.

Loh, K.M., and Lim, B. (2011). A precarious balance: pluripotency factors as lineage specifiers. *Cell Stem Cell* 8, 363–369.

Loos, R.J., and Yeo, G.S. (2014). The bigger picture of FTO-the first GWAS-identified obesity gene. *Nat. Rev. Endocrinol.* 10, 51–61.

Meyer, K.D., and Jaffrey, S.R. (2014). The dynamic epitranscriptome: N6-methyladenosine and gene expression control. *Nat. Rev. Mol. Cell Biol.* 15, 313–326.

- Meyer, K.D., Saletore, Y., Zumbo, P., Elemento, O., Mason, C.E., and Jaffrey, S.R. (2012). Comprehensive analysis of mRNA methylation reveals enrichment in 3' UTRs and near stop codons. *Cell* **149**, 1635–1646.
- Montserrat, N., Nivet, E., Sancho-Martinez, I., Hishida, T., Kumar, S., Miquel, L., Cortina, C., Hishida, Y., Xia, Y., Esteban, C.R., and Izpisua Belmonte, J.C. (2013). Reprogramming of human fibroblasts to pluripotency with lineage specifiers. *Cell Stem Cell* **13**, 341–350.
- Neff, A.T., Lee, J.Y., Wilusz, J., Tian, B., and Wilusz, C.J. (2012). Global analysis reveals multiple pathways for unique regulation of mRNA decay in induced pluripotent stem cells. *Genome Res.* **22**, 1457–1467.
- Niu, Y., Zhao, X., Wu, Y.S., Li, M.M., Wang, X.J., and Yang, Y.G. (2013). N6-methyl-adenosine (m6A) in RNA: an old modification with a novel epigenetic function. *Genomics Proteomics Bioinformatics* **11**, 8–17.
- Rahl, P.B., Lin, C.Y., Seila, A.C., Flynn, R.A., McCuine, S., Burge, C.B., Sharp, P.A., and Young, R.A. (2010). c-Myc regulates transcriptional pause release. *Cell* **141**, 432–445.
- Schnerch, A., Cerdan, C., and Bhatia, M. (2010). Distinguishing between mouse and human pluripotent stem cell regulation: the best laid plans of mice and men. *Stem Cells* **28**, 419–430.
- Schwartz, S., Agarwala, S.D., Mumbach, M.R., Jovanovic, M., Mertins, P., Shishkin, A., Tabach, Y., Mikkelsen, T.S., Satija, R., Ruvkun, G., et al. (2013). High-resolution mapping reveals a conserved, widespread, dynamic mRNA methylation program in yeast meiosis. *Cell* **155**, 1409–1421.
- Schwartz, S., Mumbach, M.R., Jovanovic, M., Wang, T., Maciag, K., Bushkin, G.G., Mertins, P., Ter-Ovanesyan, D., Habib, N., Cacchiarelli, D., et al. (2014). Perturbation of m6A writers reveals two distinct classes of mRNA methylation at internal and 5' sites. *Cell Rep.* **8**, 284–296.
- Segal, E., Shapira, M., Regev, A., Pe'er, D., Botstein, D., Koller, D., and Friedman, N. (2003). Module networks: identifying regulatory modules and their condition-specific regulators from gene expression data. *Nat. Genet.* **34**, 166–176.
- Sharova, L.V., Sharov, A.A., Nedorezov, T., Piao, Y., Shaik, N., and Ko, M.S. (2009). Database for mRNA half-life of 19 977 genes obtained by DNA microarray analysis of pluripotent and differentiating mouse embryonic stem cells. *DNA Res.* **16**, 45–58.
- Shu, J., Wu, C., Wu, Y., Li, Z., Shao, S., Zhao, W., Tang, X., Yang, H., Shen, L., Zuo, X., et al. (2013). Induction of pluripotency in mouse somatic cells with lineage specifiers. *Cell* **153**, 963–975.
- Sibbritt, T., Patel, H.R., and Preiss, T. (2013). Mapping and significance of the mRNA methylome. *Wiley Interdiscip. Rev. RNA* **4**, 397–422.
- Sigova, A.A., Mullen, A.C., Molinie, B., Gupta, S., Orlando, D.A., Guenther, M.G., Almada, A.E., Lin, C., Sharp, P.A., Giallourakis, C.C., and Young, R.A. (2013). Divergent transcription of long noncoding RNA/mRNA gene pairs in embryonic stem cells. *Proc. Natl. Acad. Sci. USA* **110**, 2876–2881.
- Trapnell, C., Pachter, L., and Salzberg, S.L. (2009). TopHat: discovering splice junctions with RNA-Seq. *Bioinformatics* **25**, 1105–1111.
- Ulitisky, I., Shkumatava, A., Jan, C.H., Sive, H., and Bartel, D.P. (2011). Conserved function of lincRNAs in vertebrate embryonic development despite rapid sequence evolution. *Cell* **147**, 1537–1550.
- Wang, X., Lu, Z., Gomez, A., Hon, G.C., Yue, Y., Han, D., Fu, Y., Parisien, M., Dai, Q., Jia, G., et al. (2014a). N6-methyladenosine-dependent regulation of messenger RNA stability. *Nature* **505**, 117–120.
- Wang, Y., Li, Y., Toth, J.I., Petroski, M.D., Zhang, Z., and Zhao, J.C. (2014b). N6-methyladenosine modification destabilizes developmental regulators in embryonic stem cells. *Nat. Cell Biol.* **16**, 191–198.
- Wong, D.J., Liu, H., Ridky, T.W., Cassarino, D., Segal, E., and Chang, H.Y. (2008). Module map of stem cell genes guides creation of epithelial cancer stem cells. *Cell Stem Cell* **2**, 333–344.
- Young, R.A. (2011). Control of the embryonic stem cell state. *Cell* **144**, 940–954.
- Zheng, G., Dahl, J.A., Niu, Y., Fedorcsak, P., Huang, C.M., Li, C.J., Vågbo, C.B., Shi, Y., Wang, W.L., Song, S.H., et al. (2013). ALKBH5 is a mammalian RNA demethylase that impacts RNA metabolism and mouse fertility. *Mol. Cell* **49**, 18–29.